Repairing surface defects of metal parts by groove machining and wire + arc based filling

Li, Yongzhe; Han, Qinglin; Horvath, Imre; Zhang, Guangjun

DOI
10.1016/j.jmatprotec.2019.116268

Publication date
2019

Document Version
Accepted author manuscript

Published in
Journal of Materials Processing Technology

Contents lists available at ScienceDirect

Journal of Materials Processing Tech.

journal homepage: www.elsevier.com

Repairing surface defects of metal parts by groove machining and wire + arc based filling

Yongzhe Li [a, b], Qinglin Han [a], Imre Horváth [b], Guangjun Zhang [a, *]

[a] State Key Laboratory of Advanced Welding and Joining, Harbin Institute of Technology, 150001, Harbin, China
[b] Faculty of Industrial Design Engineering, Delft University of Technology, 2628 CE, Delft, the Netherlands

ARTICLE INFO

Associate Editor: E. Budak

Keywords:
Metal part repair
Surface defects
Groove machining
Wire and arc additive manufacturing
Design principles
Hybrid manufacturing

ABSTRACT

An approach to repairing surface defects of metal parts is proposed, which includes a combined application of (i) groove machining, (ii) wire and arc additive manufacturing (WAAM), and (iii) finishing machining. The completed analysis revealed that (i) the inclination angle of the groove to be machined is strongly influenced by the manufacturing parameters of the WAAM process, and (ii) the WAAM process models designed for fabricating parts on a flat substrate are not appropriate for filling grooves. To overcome these issues, this research investigated the range of variation of the proper inclination angle of the groove. A mathematical model was developed to determine the manufacturing parameters of WAAM that result in a proper filling of the groove. The effectiveness of the proposed fundamentals was investigated in a case study. The experimental results showed that using the proposed approach and the chosen manufacturing parameters resulted in a complete filling of the machined groove. The fabrication error of the main part of the repaired region before the finishing machining was less than 0.3 mm, while the 'buy-to-fly' ratio of the deposited material was 92.1%. The proposed approach for morphological repair lends itself to a computer-aided automatic part repair process.

1. Introduction

1.1. Setting the stage

Millions of large-volume metal parts are fabricated and utilized in the industry every year. Contrary to the applied advanced technologies, various defects may occur either in the fabrication of the parts or be caused in operation by overload or heavy duty. Generally, two types of defects can be differentiated, including 'morphological defects' and 'structural defects'. This study dealt with morphological defects only, which typically include holes, cracks, segregation, inclusions, surface marks, and notches (Wilby and Neale, 2009). Morphological defects of parts may be caused by applied shape-forming process, such as blowhole, sand burning, and sand inclusion defects on casting parts (Rajkolhe and Khan, 2017). Defects may also be produced in the process of materials processing, such as pores and cracks created by grinding and polishing (Zhang et al., 2006). Furthermore, Chen et al. (2014) claimed that defects may be generated on auxiliary process equipment, such as defects on forging dies. Morphological defects normally appear on the surface of parts (*i.e.* surface defects), which may reduce the performance of the parts in operation and may lead the parts to be scrapped. For interplaying safety, economic, technological, and business reasons, the need for part repair has emerged in the industry a long time ago. Despite the long existing need, even nowadays, the manual repair is still the most commonly used approach in the industrial practice. For instance, worn parts are repaired by manual shield metal arc welding (Lant et al., 2001) and the superfluous material is removed by hand grinding and polishing (Pikuła et al., 2017). Therefore, the development of flexible, powerful and economic repair technologies and techniques have become an important topic for scientific research as well as for industrial investigations (Yu et al., 2018).

1.2. Related works and results

Hybrid manufacturing (HM) was considered for part repair more than ten years ago (Ren et al., 2007). HM combines subtractive manufacturing (SM) processes, which were applied to remove undesirable material from a part, and additive manufacturing (AM) processes,

Abbreviations: WAAM, wire and arc additive manufacturing; AM, additive manufacturing; SM, subtractive manufacturing; HM, hybrid manufacturing; MSA, material shortage areas.

* Corresponding author at: State Key Laboratory of Advanced Welding and Joining, Harbin Institute of Technology, No. 92, West Da-Zhi Street, Harbin, Heilongjiang, 150001, China.
Email addresses: y.li-8@tudelft.nl (Y. Li); hanqinglin2014@163.com (Q. Han); I.Horvath@tudelft.nl (I. Horváth); zhanggj@hit.edu.cn (G. Zhang)

https://doi.org/10.1016/j.jmatprotec.2019.116268
Received 12 December 2018; Received in revised form 12 May 2019; Accepted 16 June 2019
Available online xxx
0924-0136/

which were used for rebuilding the missing material of the part according to its CAD model. Most of the existing HM-based part repair systems rely on laser-based AM technologies. For instance, Yilmaz et al. (2010) proposed a methodology for repair and maintenance of aero-engine components via reverse engineering, laser-based welding, and machining. Penaranda et al. (2017) reported an adaptive laser cladding approach for repairing blade tip. However, this type of systems did not become widespread in the industry due to the expensive equipment and the complex installation (Wang et al., 2002).

Wire and arc additive manufacturing (WAAM) has been recognized as a promising solution for part repair owing to the simple and low-cost equipment (Williams et al., 2016). As a technology, WAAM is able to produce full-density components that are made of various materials (Ding et al., 2015b). For instance, Xiong et al. (2017) proposed a method for fabrication of inclined thin-walled steel parts by using GMAW. The system implemented by Horgar et al. (2018) was able to produce parts made of AA5183 aluminium alloy. Recently, Wu et al. (2018) applied an inter-pass cooling process to fabricate Ti6Al4V thin-walled structures by using GTAW. The typical disadvantages of using welding arc as the heat source in additive manufacturing have been identified as local metallurgical changes, shape distortion, and residual stress concentration (Knezović and Topić, 2018). Many innovative solutions are reported in the literature to deal with these issues. For instance, to reduce the amount of heat input in deposition, Chen et al. (2018) implemented a cold metal transfer (CMT) welding - based system to fabricate inclined aluminum parts. Bermingham et al. (2018) employed articulated post process treatments to enhance the mechanical properties of WAAM fabricated components. Moreover, Hönnige et al. (2018) made use of vertical inter-pass rolling to eliminate distortions of WAAM parts.

A number of WAAM-based HM implementations were brought to the existence and used in the academic and industrial practice in the last decade. For instance, Song et al. (2005) reported on a system that combines gas metal arc welding (GMAW) and 3D milling to fabricate simple parts. Karunakaran et al. (2009) used a pulsed synergic GMAW machine and a commercial 3-axis CNC machine tool to automatically fabricate complex metal parts with high geometric accuracy. Panchagnula and Simhambhatla (2016) used a CMT welding machine and a CNC milling center with 3-linear and 2-rotary axes to produce overhanging metal parts. Ding et al. (2016) integrated WAAM and milling to fabricate metal parts from CAD models in an automatic manner. An important finding is that the majority of the currently known WAAM-based HM implementations aims at direct fabrication of parts on a flat substrate, but has not yet been tailored to part repairing. Consequently, the solutions proposed so far have several limitations in repairing parts with significant morphological defects such as surface cracks, deep pores, and scale pits.

1.3. The objectives and contents of this paper

The objective of this paper is to elaborate on the fundamentals of repairing metal parts with morphological defects concerning geometrical requirements. As the first step in the repair process, the identified individual or interrelated multiple surface defects should be removed from a concerned part by using a dedicated material removal procedure, which converts the arbitrarily shaped surface defects into one or more grooves with a regular shape. Every groove is a minimum volume (concave) void and is formed so as to facilitate the material depositing process. The deposition involves positioning and laying multiple beads according to a tailored process plan. Following the groove-filling procedure, the extra deposited material should be removed and the nominal shape of the part should be produced as precisely as possible or required.

As mentioned above, WAAM was considered in the work as a space-filling/material deposition technology. In this context, several specific issues should be addressed and resolved. On the one hand, geometries (*e.g.* inclination angle) of a groove should be determined before applying a machining operation. This fact implies a research question regarding what geometries are able to support bead deposition/filling, and prevent the formation of voids between the groove and the deposited material. On the other hand, no mathematical model has been proposed in the literature yet for planning the WAAM-based groove-filling process, and for calculating the manufacturing parameters for depositing in a groove. Likewise, no principles or rules have been published concerning the morphological design of the groove and achieving an optimal result in repair. Actually, these were the research challenges for the partly theoretical, partly practical work reported in this paper.

The content of this paper is organized as follows: Section 2 provides a concise overview of the overall repair process. Based on this, specific research questions are defined. Section 3 deals with the procedural aspects of the proposed approach. The first sub-section discusses the mathematical model for calculating the manufacturing parameters of the WAAM-based deposition in a groove, whilst the second sub-section analyses the allowed range (actually the end limits) of the inclination angle of the side surfaces of the groove considering its effect on the bead formation. Section 4 presents the technical details of a case study conducted with the aim of validation. Section 5 discusses the experimental results of the case study and the major findings from the experimental results. Finally, Section 6 proposes the conclusions of this research.

2. An overview of the repair process of surface defects

2.1. Basic concepts and assumptions

Various kinds of grooves have been considered in the research projects reported in the literature with regard to metal part repairs, such as circular truncated cones (Liu et al., 2014), V-shaped groove (Branza et al., 2009) and U-shaped groove (Graf et al., 2012). Due to the possible geometric diversity of parts to be repaired and to the complexity of possible defects, there is still no agreement in the literature regarding what kind of concave groove (*e.g.* shape, geometries) is the best. For the sake of simplicity, the investigation of this paper is based on the following assumptions. Firstly, a rectangular base shape provides optimum conditions for depositing weld beads. In addition, the groove generated by the machining operations can be a pyramidal frustum with two rectangular bases. Based on these assumptions, three statements can be derived. Morphological defects should appear on a flat surface of a part. The two bases of the groove should preferably be parallel. And then, every layer sliced from the groove can be of a uniform thickness. It is worth mentioning that the proposed assumptions are made because of a technical simplification for investigating the fundamentals, rather than because of a theoretical or methodological limitation. The technical solutions proposed based on these assumptions are transferable and can be considered as a basis for complex cases.

Keeping the above considerations and preliminaries in mind, the groove physically relevant to any surface defects has been conceptualized as a pyramidal frustum with a flat bottom surface and slanted side surfaces, and is symbolically described as a quintuple, GO:{L_b,W_b,D_g,α,β}, where: GO stands for a groove, and L_b is the length of the base plane of GO in the longitudinal direction, W_b is the width of the base plane of GO in the transversal direction, D_g is the groove depth measured between the upper and the lower base planes (the nominal height of the void) of GO in normal direction, α is the acute tilting angle of the longitudinal side (lateral) surfaces relative to the surface extension of the base plane, and β is the acute tilting angle of

the traversal side surfaces relative to the surface extension of the base plane. Apart from special cases, the assumption that $\alpha = \beta = \theta$ applies. θ is the generic inclination angle of the groove.

2.2. The phases of a WAAM-centered repair process

Based on the above assumptions, the general workflow of repairing parts by groove machining, WAAM and finishing machining is shown in Fig. 1. There are three operational steps, including step 1 – using machining operations to chip off the concerned defects from the target part, based on which a pyramidal frustum (the groove) is formed; step 2 – using WAAM operations to deposit materials in a layer-by-layer manner to fill the groove properly; and step 3 – using machining operations again to remove the redundant materials in order to reduce the surface unevenness and to increase the fabrication accuracy. In the literature, many solutions have been reported to support step 3 (the finishing machining operations), such as the works surveyed in Flynn et al. (2016). For the above reason, this paper focuses on steps 1 and 2, exclusively.

The basic requirement for the first machining operation is to form a suitable concave groove for bead depositing by the WAAM system. The suitability of the groove is considered from two aspects. On one hand, the geometry of the groove should guarantee that the surface of the groove is fully fused with the weld beads deposited in the WAAM process. On the other hand, the weld gun used by the WAAM system should be able to access the preplanned working positions in the groove. As an implication of the proposed assumptions, the width and the length of the lower base, as well as the depth of the groove, are normally determined according to the actual size of concerned defects (to be chipped off). The inclination angle of the groove should be carefully designed to satisfy the basic requirement.

Every layer deposited by WAAM in a groove should achieve a certain preplanned height. If a groove with a small inclination angle is machined, as shown in Fig. 2, in order to reach the expected height of the layer, the weld bead deposited at the boundary of the lower base should melt the lateral face with a relatively long distance. However, the weld bead is normally solidified from weld pool within a short period of time and it may not have enough heat to melt a great amount of material belonging to the groove. Accordingly, the actual toe of the deposited weld bead (*i.e.* the point E' in Fig. 2) may be lower than the position where it is expected to reach (*i.e.* the point E in Fig. 2). In this situation, an incomplete fusion is formed on the lateral face of the groove, as indicated by the circle in Fig. 2. On the other hand, if a large inclination angle is applied to the groove, the weld gun may collide with the part. In other words, since the weld gun has a volume, it may not be able to reach the working positions. Therefore, the inclination angle of the groove should be determined according to the manufacturing parameters of the WAAM process.

The basic requirement for the WAAM operation is to fill the machined groove as precisely as possible. The basis of planning can be a descriptive mathematical model (e.g. beads-overlapping and layers-overlapping models). However, it is important to mention that the mathematical models used in the existing WAAM implementations are designed for direct fabrication of parts on a flat substrate. For instance, Li et al. (2018a) proposed a layers-overlapping model for fabrication of multi-layer multi –bead (MLMB) cuboid parts. Li et al. (2018b) reported a method for fabrication of inclined MLMB parts on a flat substrate. Therefore, these descriptive models cannot be used directly in case of part repair. The obvious reason is that the layers to be fabricated in a groove have supportive lateral surfaces, while these are not considered at depositing on a flat substrate. If the existing geometric and process models are applied to deposit weld beads in a groove, as shown in Fig. 3, material shortage areas (MSAs) may be generated at the edges of the layers. Although the generated MSAs could be compensated by depositing an additional amount of material for the weld beads belonging to the upper layers, incomplete fusions may happen at the toes of the layers, as indicated by the circles in Fig. 3, for the reason that these places are far away from the source of heat (*i.e.* the welding arc), as indicated by the arrow in Fig. 3.

The definition of the research problems and the general description of the repair process entails that the manufacturing parameters for AM operations and SM operations are interrelated. On the one hand, it should be considered whether the inclination angle of the groove ma-

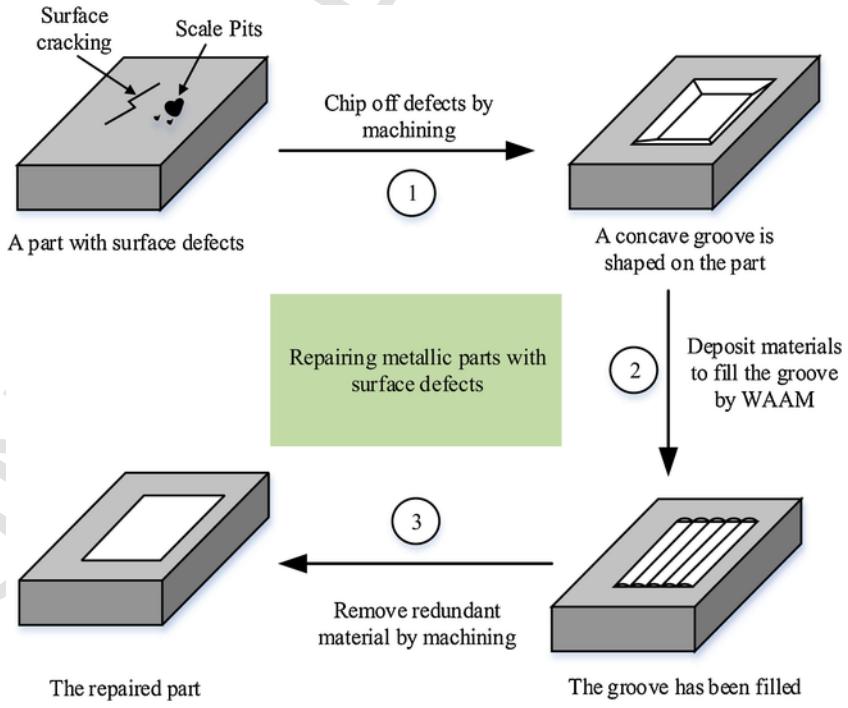

Fig. 1. The workflow of repairing parts with surface defects based on machining and WAAM.

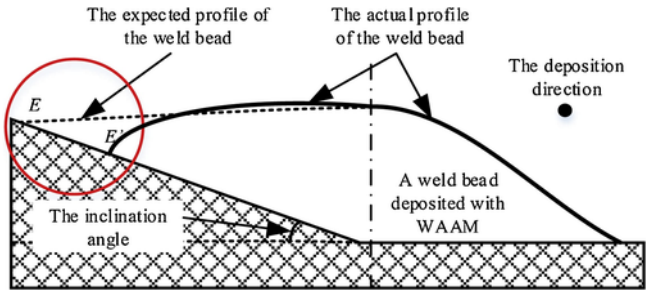

Fig. 2. The technical issue caused by machining a groove with a small inclination angle.

chined by the chosen SM operation is suitable for deposition of weld beads by the chosen AM operation. On the other hand, the manufacturing parameters applied to specify the AM process should be determined according to the geometries of the groove, which are shaped by the SM operation. Therefore, the manufacturing parameters for both operations should be jointly designed.

3. Construction of a mathematical model

3.1. Modeling the deposition of beads in a groove

As mentioned in the previous section, below a new mathematical model for WAAM is proposed that facilitates the fabrication of layers with supportive lateral surfaces. This model incorporates a rudimentary model of the cross-sectional profile of a layer to be deposited in a groove by WAAM, which is shown in Fig. 4. In the model, the geometries (*i.e.* height and width) of the elementary weld beads were considered to be the same in each layer. Then, the width of the bottom of the layer (or the lower base of the groove) can be computed as follows:

$$W_b = (n-1)d_b + 2d_o \tag{1}$$

where: W_b is the width of the bottom of the layer, w is the width of a single weld bead, d_b is the distance between adjacent weld beads in the layer, a is the step-over rate and $d_b = aw$, n is the number of weld beads contained in the layer, d_o is the offset distance between the boundary of the bottom of the layer and the deposition position of the first bead (or the last bead) in the layer.

The height of the layer, H, is defined as the average height of the main body of the layer, which is the overlapped part of two adjacent beads. As suggested in the literature, the cross-sectional profile of a single weld bead can be represented by a symmetric parabola model (Suryakumar et al., 2011). With this, the height of the layer can be calculated by the following equation:

$$H = \frac{\frac{2}{3}wh}{d_b} = \frac{2h}{3a} \tag{2}$$

where: h is the height of a single weld bead.

Introduced in the previous section, if the inclination angle of the groove is θ, then the horizontal distance between the boundary of the bottom of the layer and the bottom of the layer above on one side can be calculated as follows:

$$d_r = H/\tan\theta \tag{3}$$

Then, the upper width of the layer (which can be considered as the bottom of the layer above the concerned layer) can be calculated as:

$$W_{ab} = (n-1)aw + 2d_o + 2d_r \tag{4}$$

According to the requirement concerning the filling of the groove, the height of the two edges of the layer (*i.e.* the left half of the first bead and the right half of the last bead shown in Fig. 4) should be equal to the height of the main body of the layer. Considering the first bead in the model as an example, the area of the quadrangle OPQR should be equal to the sum of the area S_1 and S_2, which can be calculated by the following equation:

$$S_{OPQR} = \frac{2h}{3a}(d_r + d_o) = S_1 + S_2 \tag{5}$$

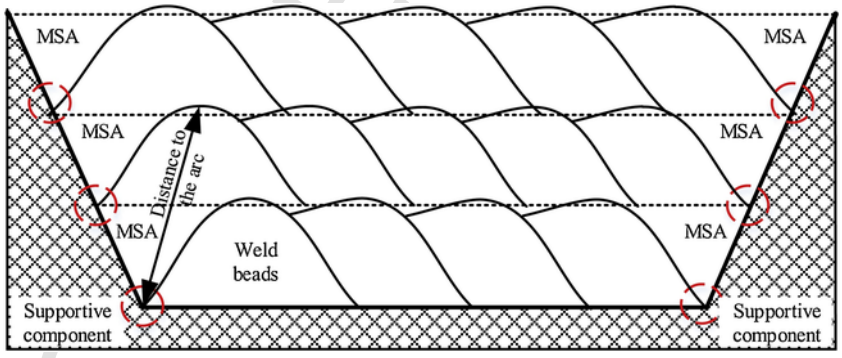

Fig. 3. The technical issues caused by applying the existing process model for depositing materials in a given groove.

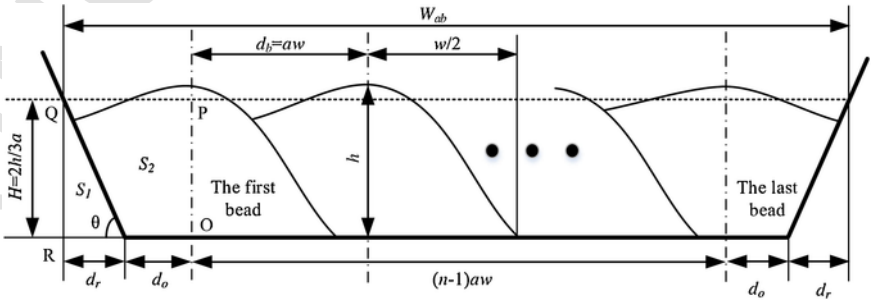

Fig. 4. The cross-sectional profile of a layer to be deposited in a groove.

where: S_1 and S_2 are calculated as:

$$S_1 = hd_r/3a \tag{6}$$

and,

$$S_2 = wh/3 \tag{7}$$

Taking Eqs. (5)–(7) into consideration, the following equation can be obtained:

$$d_r + 2d_o = wa \tag{8}$$

Based on Eqs. (2), (3) and (8), the following equation can be obtained:

$$d_o = \frac{wa}{2} - \frac{h}{3a\tan\theta} \tag{9}$$

Furthermore, based on Eqs. (1) and (9), the following equation can be obtained.

$$w = \frac{W_b + \frac{2h}{3a\tan\theta}}{na} \tag{10}$$

Eqs. (1)–(10) provide the information necessary to calculate the process parameters for filling a groove by WAAM. For a given groove (for which W_b and tanθ are known), Eq. (2) can be applied to calculate the height of an elementary bead in the layer when the step-over rate between adjacent beads, a, and the height of a layer, H, are determined. Then, Eq. (10) can be used to calculate the relation between the number of beads in the layer, n, and the width of the beads contained in the layer, w. Since n is an integer, alternative widths can be calculated when different n are considered. This means that the most suitable width should be selected from the alternatives that can be produced by the WAAM system. After the width of the elementary weld in the layer is specified, Eq. (9) can be applied to calculate the deposition position of the first bead (and the last bead) in the layer. Then, the deposition positions of the rest weld beads in the layer can be calculated by applying the specified step-over distance ($d_b = wa$). After the concerned layer is deposited, Eq. (4) can be used to calculate the width of the above layer and the geometries of the elementary beads belonging to the above layer are to be computed. In this way, the deposition of multiple overlapping layers can be realized.

3.2. Determining the allowed range of inclination angle of the groove

It can be seen based on the process model developed for the WAAM process that the inclination angle of the groove and the geometries of the elementary weld beads are interrelated. This implies that the allowed range of the inclination angle in the fabrication of the groove is associated with the geometries of the beads. In the following part, the lower limit and the upper limit of the inclination angle are discussed separately, which define the allowed range to be achieved by machining. The geometric model of the cross-sectional profile of the first bead deposited in a groove is shown in Fig. 5. Based on the coordinate system used in this figure, the coordinates of point E, which is the toe of the bead formed on the lateral face of the groove, are (x_E, y_E). Since point E is on the line BE, the following equation can be derived:

$$y_E = -\frac{H}{d_r}(x_E + d_o) \tag{11}$$

where: $d_r > 0$ and $d_o > 0$.

If the curve AE is simplified to be a straight line, as recommended by Ding et al. (2015a), the equation of line AE is as follows:

$$y = \frac{(x - x_E)(y_E - h)}{x_E} + y_E \tag{12}$$

Accordingly, the area enclosed by the points AEBO can be calculated by the following equation:

$$S_{AEBO} = S_{EJB} + S_{JBOA} = \frac{d_o y_E - x_E h}{2} \tag{13}$$

Since the area of AEBO is half of the area of a single weld bead, the following equation can be derived:

$$\frac{d_o y_E - x_E h}{2} = \frac{wh}{3} \tag{14}$$

Then, based on Eqs. (11) and (14), x_E can be expressed as:

$$x_E = -\frac{2awd_r + 2d_0^2}{2d_0 + 3ad_r} \tag{15}$$

If the weld bead is deposited on a flat substrate, then the cross-sectional profile of the bead can be assumed to be represented by the dashed line shown in Fig. 5. In this situation, the left toe of the weld bead is located at point F. In the considered system of coordinates, the position of point F is $(-w/2, 0)$. When the lateral face is taken into consideration, the weld pool will melt some material of the lateral face. As a result, a portion of the heat of the weld pool for shaping the weld bead may dissipate through the lateral face. This heat dissipation in turn reduces the solidification time of the weld pool. For this reason, it can be argued that the horizontal position of point E should be on the right of that of point F. This relationship can be represented as an inequality of the following form:

$$x_E > -w/2 \tag{16}$$

Based on Eqs. (15) and (16), the following result can be obtained.

$$\tan\theta > \tan\theta_{min} = \frac{4h}{3aw(\sqrt{2a + 1 - 3a^2} + a - 1)} \tag{17}$$

The upper limit of the range of the inclination angle of the fabricated groove should consider the accessibility of the weld gun to the working positions. In this work, the flat-position deposition was considered as the welding posture since it is the basis for using the symmetrical parabola model to represent the cross-sectional profile of a single weld bead. In this situation, the stick-out distance of the weld gun should be considered, which is defined as the vertical distance between the weld gun and the expected working positions in the groove. If the depth of the groove is bigger than the stick-out distance, the weld gun should be put into the groove to complete the deposition processes. The upper limit of the range of the inclination angle of the groove is shown in Fig. 6. Based on the geometric relationships, the following constraint can be derived:

$$\tan\theta < \tan\theta_{max} = \frac{d_{so}}{\frac{d_{gun}}{2} - d_o} \tag{18}$$

where: d_{gun} is the diameter of the weld gun, and d_{so} is the stick-out distance. According to the literature, the stick-out distance influences the

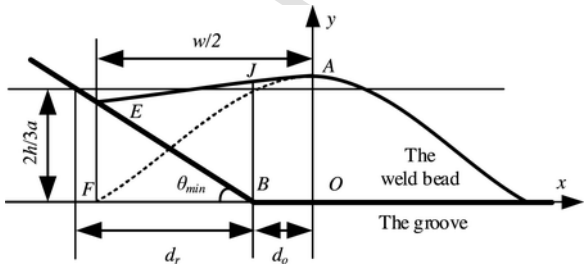

Fig. 5. The lower limit of the range of the inclination angle of the groove.

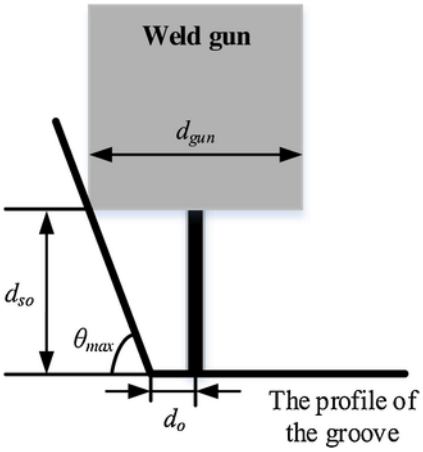

Fig. 6. The upper limit of the range of the inclination angle.

geometries of the deposited weld bead (Xiong et al., 2014). It means that normally d_{so} and d_{gun} become definitive when the geometries of the weld beads have been determined.

By combining Eqs. (18) and (9), the following constraint can be derived:

$$\tan\theta < \frac{2d_{so}-H}{d_{gun}-wa} \tag{19}$$

Therefore, the allowed fabrication range of the inclination angle of a groove to be machined can be specified by the following constraints:

$$\begin{cases} \frac{4h}{3aw(\sqrt{2a+1-3a^2}+a-1)} < \tan\theta < \frac{2d_{so}-\frac{2h}{3a}}{d_{gun}-wa} & , d_{so} \le D_g \\ \frac{4h}{3aw(\sqrt{2a+1-3a^2}+a-1)} < \tan\theta & , d_{so} > D_g \end{cases} \tag{20}$$

where: D_g is the depth of the fabricated groove.

From Eq. (20) it can be seen that the lower limit of *tanθ* is associated with the height to width ratio of the elementary weld bead, h/w, and the step-over rate, a, applied to arrange the weld beads in the layer. In order to reduce the unevenness of the layer surface, a is normally predefined and constant. The h/w of the elementary weld beads is the only factor that influences the lower limit of *tanθ*. As the h/w increases, the lower limit of tanθ also increases. Similarly, the upper limit of tanθ increases, if w increases and/or h decreases. What it means is that a relatively low h/w should be considered at determining the geometries of the weld beads for filling a groove. Should this be the situation, then the lower limit of the fabrication range is relatively small, while the upper limit of the fabrication range is relatively large. These together provide more room for determining the actual inclination angle at shaping the groove.

As an intermediate conclusion, Eqs. (1)–(20) describe the fundamental principles of generating the parameters for groove machining as well as for the WAAM process in the case of repairing parts having morphological (surface) defects. The details with regard to using these fundamental principles for designing the manufacturing parameters will be presented in the next section through a real-life case study. The objective of conducting this case study was to validate the feasibility of the proposed fundamental principles.

4. Application of the mathematical model in a case study

4.1. Introducing the experimental setup

The WAAM-based part repair was based on a robot-enabled GMAW system. A detailed illustration of the basic constituents of the implemented system can be found in (Li et al., 2018c). The specific settings for this case study are shown in Table 1. To validate the proposed concepts, specimens were produced for experimentation. Every specimen was a cubic thick plate, on which a groove was machined by using a Luzhong ZX6350D milling machine. According to the fundamental principles presented above, the inclination angle of the groove was determined based on the geometries of elementary weld beads applied in the deposition. It entailed that a set of basic experiments should be first done to obtain information about the possible geometries (*i.e.* height and width) of weld beads under varied experimental conditions. In the basic experiments, single weld beads were deposited on a flat substrate using the implemented WAAM system. The geometries of the flat-substrate weld beads were measured by a structured-light sensor.

The measured geometries of the deposited single weld beads are shown in Table 2. The symbol v_f stands for the wire-feeding speed and v_d for the deposition speed. The lower and upper limits of the inclination angle of the to-be-machined groove were calculated by Eq. (20). The calculated results are shown in Table 2. It can be seen that, the maximal value of tanθ was 1.245, while the minimal value of tanθ was 1.337. Since the actually machined inclination angle of the groove should satisfy the design requirements for most situations, tanθ was set to 4/3 in the experimentation. The geometries of the specimen were designed based on this, as shown in Fig. 7(a). The groove machined into the specimen was designed according to the determined inclination angle. The fabricated specimen is shown in Fig. 7(b).

4.2. Details of filling the groove by WAAM

4.2.1. Specifying the geometries of the layers and beads

The applied milling machine provided a specific machining accuracy. With a view to the realized accuracy, the geometries of the fabricated groove were individually measured using the structured-light sensor, as shown in Fig. 8. The descriptive data of the detected groove geometries are shown in Table 3. For each parameter, 20 measurements were taken and the average value was used as the detected value. The groove with these data was regarded as the actual geometries of the groove to be filled. Based on the measured geometries, 1.377 was calculated as the actual $\tan\theta_{min} < \tan\theta_r < \tan\theta_{max}$ of the machined groove.

After these measurements, the geometries of the layers and the elementary weld beads in the layers were specified. The fabricated groove was sliced into a total of four layers. The thickness of the lower three layers was set to 2.50 mm. The thickness of the top layer was determined based on the depth of the groove and some practical considerations. On the one hand, geometries of weld beads deposited by WAAM may fluctuate. It causes geometric deviations between the values expected based on the mathematical model and the shaped weld beads. In addition, no ideal flat surface could be realized at the joint of two overlapped weld beads (Ding et al., 2015a). In order to fully fill the groove, the total height achieved by the layers has to be bigger

Table 1
Experimental setup values for the case study.

Material of substrate	Material of fed-wire	Diameter of fed-wire	Shielding gas	Flow rate	Diameter of weld gun	Stick-out distance
Q235	H08Mn2Si	1.2 mm	95%Ar + 5%CO_2	18 L/min	21 mm	12 mm

Table 2
The calculated limits of tanθ in different conditions.

No.	Manufacturing parameters				Geometries of beads		Limits	
	U(V)	v_f (m/min)	v_d (mm/s)	a	h (mm)	w (mm)	tanθ	tanθ
1	24.0	3.73	6.0	0.738	2.11	7.83	0.742	1.452
2	21.5	3.73	6.0	0.738	2.46	7.04	0.962	1.378
3	21.5	2.76	6.0	0.738	2.03	6.06	0.922	1.341
4	23.0	3.16	7.2	0.738	1.89	6.59	0.790	1.382
5	20.0	4.31	4.8	0.738	2.96	8.20	0.994	1.427
6	21.5	3.73	6.0	0.738	2.42	7.14	0.936	1.386
7	21.5	3.73	8.0	0.738	2.09	6.11	0.943	1.341
8	23.0	4.31	4.8	0.738	2.85	9.09	0.862	1.500
9	21.5	3.73	6.0	0.738	2.40	7.13	0.928	1.387
10	23.0	3.16	4.8	0.738	2.31	7.92	0.805	1.446
11	21.5	3.73	6.0	0.738	2.26	7.51	0.830	1.420
12	20.0	3.16	7.2	0.738	2.12	6.08	0.960	1.337
13	21.5	4.93	6.0	0.738	2.72	8.70	0.862	1.478
14	19.0	3.73	6.0	0.738	2.45	6.67	1.013	1.355
15	20.0	4.31	7.2	0.738	2.34	7.36	0.876	1.406
16	20.0	3.16	4.8	0.738	2.43	7.66	0.872	1.421
17	21.5	3.73	6.0	0.738	2.46	7.16	0.946	1.386
18	23.0	4.31	7.2	0.738	2.17	7.86	0.761	1.450
19	21.5	3.73	4.0	0.738	2.83	9.10	0.858	1.501
20	21.5	3.73	6.0	0.738	2.14	7.26	0.813	1.411
21	22.4	2.84	7.1	0.738	1.57	5.98	0.724	1.362
22	22.3	3.30	6.2	0.738	1.94	6.84	0.783	1.394
23	24.0	4.05	7.0	0.738	1.99	7.49	0.732	1.435
24	24.0	4.93	6.8	0.738	2.34	9.21	0.700	1.541
25	20.8	2.75	6.0	0.738	1.95	6.12	0.877	1.349
26	22.6	3.06	6.8	0.738	1.90	6.49	0.806	1.375
27	21.4	3.56	6.2	0.738	2.09	6.88	0.836	1.389
28	21.3	3.75	5.8	0.738	2.25	7.70	0.806	1.434
29	23.1	3.25	5.8	0.738	1.81	7.49	0.667	1.445
30	23.4	3.74	6.3	0.738	2.11	7.56	0.770	1.432
31	19.0	4.51	4.5	0.738	3.29	7.86	1.151	1.384
32	21.1	4.11	5.0	0.738	2.65	8.12	0.898	1.440
33	18.4	4.61	4.6	0.738	3.37	7.46	1.245	1.352
34	19.7	4.25	4.8	0.738	2.96	7.71	1.058	1.393
35	24.0	4.93	7.2	0.738	2.23	9.06	0.679	1.536
36	21.9	3.20	6.4	0.738	1.91	6.65	0.791	1.384
37	22.0	3.16	5.7	0.738	2.20	6.47	0.936	1.357
38	22.6	3.56	5.6	0.738	2.17	7.64	0.780	1.435
39	22.9	3.54	5.8	0.738	2.19	6.96	0.866	1.388
40	23.2	3.42	6.1	0.738	1.84	7.58	0.670	1.450
41	21.4	3.96	4.7	0.738	2.65	8.23	0.887	1.448
42	22.3	3.79	6.1	0.738	2.10	8.10	0.714	1.471
43	22.4	3.86	6.1	0.738	2.11	8.33	0.699	1.487
44	21.8	3.20	6.0	0.738	1.97	6.91	0.786	1.397
45	21.0	3.51	6.1	0.738	2.18	7.09	0.847	1.397
46	19.3	3.84	6.2	0.738	2.32	7.13	0.895	1.392
47	21.7	3.66	6.2	0.738	2.08	7.32	0.782	1.419
48	21.9	3.89	5.9	0.738	2.21	7.73	0.788	1.439
49	22.3	3.95	5.6	0.738	2.24	7.94	0.776	1.452
50	21.5	4.02	5.2	0.738	2.35	8.04	0.807	1.452

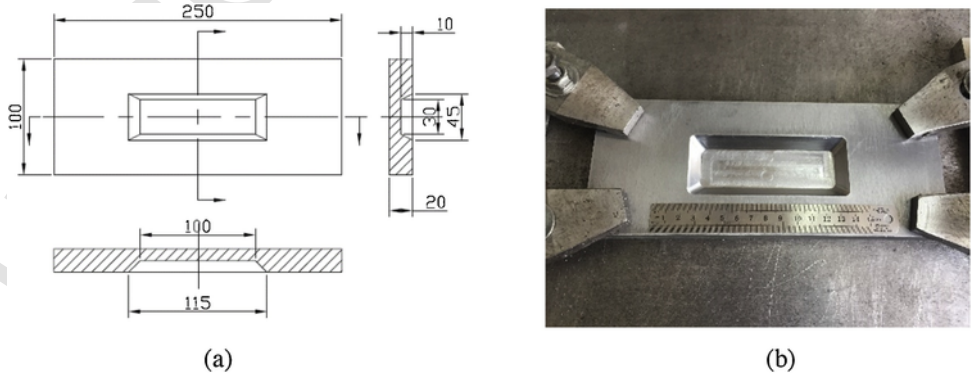

Fig. 7. The specimen with a groove shaped by machining: (a) geometries of the specimen (unit: mm) (b) the fabricated specimen.

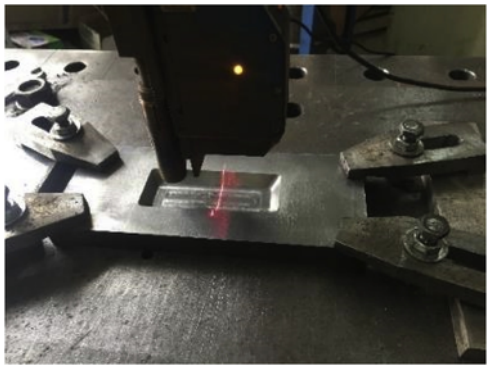

Fig. 8. Obtaining the geometries of the groove by using the structured-light sensor.

Table 3
The measured geometries of the machined groove.

Width of the lower base (mm)	Length of the lower base (mm)	Depth (mm)	Width of the upper base (mm)	Length of the upper base (mm)	The actually shaped tanθ
29.69	99.62	9.94	44.13	114.40	1.377

than the depth of the groove. The redundant height was regarded as a manufacturing allowance. In this case study, the manufacturing allowance was set to 0.5 mm. Therefore, considering the total depth of the groove and the thickness of the previously deposited three layers, the height of the top layer was set to 2.94 mm. After the specification of the layer thicknesses, the widths of the layers were determined. The calculated results are shown in Table 4.

Then, the geometries of the weld beads deposited in the layers and the manufacturing parameters used for planning the deposition paths were calculated. It also included the determination of the step-over rate to be applied between adjacent weld beads. According to the findings in the related work, the optimal step-over rate should be 0.738 to enable a stable overlapping of multiple layers (Ding et al., 2015a), and it should be 0.667 to reduce the surface unevenness of a layer (Xiong et al., 2013a). Therefore, the step-over rate for the lower three layers was set to 0.738, while that of the top layer was set to 0.667. Using the above-specified step-over rates, the heights of the elementary weld beads contained in the layers were calculated by Eq. (2). As indicated by Eq. (10), the width of the elementary weld beads in a layer depends on how many beads are included in the layer. Alternative solutions for forming the shape of the layers were calculated, which are shown in Table 4. Actually, a solution should be selected from the alternatives and applied for fabricating the layers. The principles for the selection can be explained as follows.

Firstly, for each of the solutions, the limits of tanθ should be calculated. The inclination angle of the machined groove should be in the interval calculated based on the geometries of weld beads (*i.e.* $\tan\theta_{min} < \tan\theta_r < \tan\theta_{max}$). For instance, the number of weld beads in the first layer should not be chosen to be 6, since in this situation $\tan\theta_{max} > \tan\theta_r$. In addition, the selected geometries of weld beads should be producible by using the implemented WAAM system. According to the parameters shown in Table 2, the fabrication range of the width of a weld bead (that can be produced by the used WAAM system) was specified as $5.98\ \text{mm} \le w \le 9.21\ \text{mm}$. It means that the selected widths of the weld beads should be in this range. For instance, the number of weld beads in the first layer should not be selected as 4, since the implemented system cannot deposit a weld bead with a width of 10.67 mm. Furthermore, to decrease the number of striking and distinguishing points of the welding arc, the number of weld beads in a layer should be as small as possible. According to these principles, the numbers of weld beads from the bottom layer to the top layer were determined as 5, 6, 6 and 7, respectively. Based on the numbers of weld beads in the layers, the widths of the weld beads in the layers can be specified.

4.2.2. *Predicting manufacturing parameters for depositing the weld beads*

After the geometries of weld beads were specified, the manufacturing parameters applied for depositing the weld beads should be predicted. In this case study, the prediction was done based on an algorithm implemented in the previous work. The algorithm contained a forward artificial neural network model and a reverse artificial neural network model. A detailed explanation with regard to the algorithm can be found in (Xiong et al., 2013b). Based on the algorithm, the predicted manufacturing parameters are shown in Table 5.

Then, the predicted manufacturing parameters were validated. The validation experiments were done by using the predicted parameters to deposit single weld beads on a substrate, as shown in Fig. 9. The actual geometries of the deposited single weld beads were measured by using the structured-light sensor. A comparison between the expected geometries of the weld beads for the repairing work and those of beads deposited by using the predicted manufacturing parameters is shown in Table 5. It can be seen that the maximum error of width was 0.35 mm (3.83%), while that of height was −0.13 mm (−4.69%). Therefore, the predicted manufacturing parameters can be applied for the repair work.

4.2.3. *The deposition process*

The calculated manufacturing parameters were applied for depositing weld beads in the machined groove, in order to validate the

Table 4
Alternative solutions calculated to form the shape of the layers.

No. of layer	Geometries of the layers			Alternative parameters for planning the deposition paths				Alternative geometries of weld beads		Limits of *tanθ*	
	W (mm)	tanθ	H (mm)	a	d_r (mm)	n	d_o(mm)	w (mm)	h (mm)	tanθ	tanθ
1	29.69	1.377	2.50	0.738	1.82	4	3.03	10.67	2.77	0.715	1.638
						5	2.24	8.54	2.77	0.894	1.463
						6	1.72	7.11	2.77	1.074	1.365
2	33.30	1.377	2.50	0.738	1.82	5	2.60	9.52	2.77	0.802	1.538
						6	2.02	7.93	2.77	0.963	1.419
						7	1.60	6.80	2.77	1.122	1.345
3	36.91	1.377	2.50	0.738	1.82	5	2.96	10.49	2.77	0.728	1.621
						6	2.32	8.75	2.77	0.872	1.478
						7	1.86	7.50	2.77	1.018	1.390
4	40.52	1.377	2.94	0.667	2.14	6	2.49	10.66	2.94	0.827	1.516
						7	1.98	9.14	2.94	0.965	1.413
						8	1.60	7.99	2.94	1.103	1.344

Table 5
Validating the predicted manufacturing parameters.

No. of layer	The expected geometries of beads		The predicted manufacturing parameters			Geometries of the deposited beads		Errors	
	w_p (mm)	h_p (mm)	U (V)	v_f (m/min)	v_d (mm/s)	w_r (mm)	h_r (mm)	err_w (%)	err_h (%)
1	8.54	2.77	21.5	4.19	4.66	8.66	2.80	1.41	1.08
2	7.93	2.77	20.2	4.25	4.98	8.07	2.87	1.77	3.61
3	8.75	2.77	23.0	4.12	4.96	8.61	2.64	−1.60	−4.69
4	9.14	2.94	22.5	4.67	4.61	9.49	2.87	3.83	−2.38

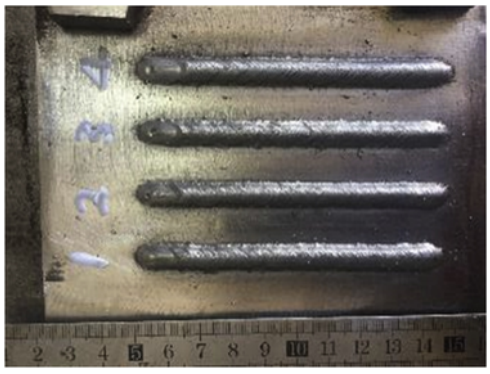

Fig. 9. The single weld beads deposited using the predicted manufacturing parameters.

feasibility of the proposed fundamentals. In addition to the calculated manufacturing parameters, the details with regard to the practical deposition process were presented as follows.

Weld beads were deposited in parallel paths, as a simplified situation to validate the proposed model. The simplification was made since the cross-sectional profiles of complex paths, *e.g.* contour and zig-zag paths, are as the same as the applied parallel paths. The overlapping of multiple weld beads is the focus of the validation, rather than the ordering of them. For every weld bead, the start position of deposition was determined according to the strategy presented in Fig. 10. The deposition started from half of d_r on the lateral face of the groove, in order to ensure the volume equivalence between the amount of the deposited material and that is needed in the groove. The same strategy was applied for determining the end positions of the depositions. Particularly, the start positions and the end positions of the weld beads belonging to the top layer were extended for 10 mm along the deposition direction, respectively. The reason for applying this strategy was to facilitate a sufficient fusion of the front and the tail boundaries of the groove with the deposited weld beads.

After a weld bead was deposited, the system waited for 2 min to prevent the part from overheating. When a layer was deposited, the beads in the next layer were deposited with a 180° rotation. It means

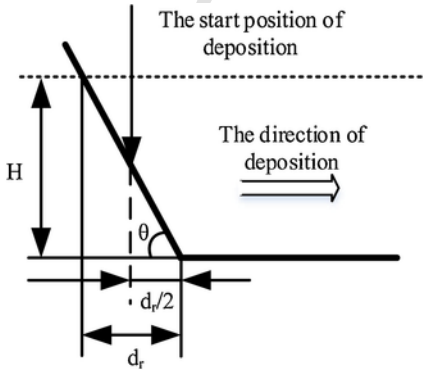

Fig. 10. The start position of arc at the front (or tail) of the groove.

that both the deposition order and the deposition direction of the weld beads were opposite to those applied in the previous layer. Due to the excavation effect of the welding arc, a weld bead in the arc striking area is high and wide, and the height of the same in the arc extinguishing area is low (Xiong et al., 2016). The reason for reversing the deposition direction was to counteract the excavation effect of the arc by overlapping the arc extinguishing areas and the arc striking areas. In addition, the reason for reversing the deposition order of the weld beads was to alleviate the residual stress concentration and to reduce the deformation of the groove as much as possible.

By using the carefully planned manufacturing parameters, the machined groove was filled. The appearance of the deposited layers is shown in Fig. 11. It can be observed that the forming appearance of the layers was reasonably good. The weld beads in the layers were uniformly distributed. The lengths of the weld beads in the layers were suitable to the length of the groove. The lateral faces of the groove were well fused with the deposited beads.

5. Discussion of the results

An image of the fabricated part is shown in Fig. 12(a), while its cross-sectional profile at the position indicated in Fig. 12(a) is presented in Fig. 12(b). It can be seen from the cross-sectional profile that the weld beads in the groove were evenly distributed. A good arrangement of the weld beads was achieved. In addition, the weld beads fused well with the boundary of the groove. No inclusion or infusion can be observed. Particularly, the two weld beads shaped at the two edges in the top layer were higher than the upper base of the groove. No gap can be observed at the edges of the upper base of the groove.

The structured-light sensor was used to detect the surface geometries of the part after the groove was completely filled. The results of the measurements are presented in Fig. 13. It can be seen that the height of the deposited material was higher than the height of the upper base of the groove. It means that the machined groove was fully filled. In addition, in the parameters planning phase, the sum of the planned heights of the layers was 0.5 mm bigger than the depth of the groove. It means that the expected height of the surface to be achieved by WAAM was planned to be 0.5 mm higher than the surface of the part. The planned height is indicated by the dashed line in Fig. 13.

It can be observed that the actual height with regard to the main body of the surface was lower than the expected height. Except for the starting and the ending sections, the fabrication error of the main body part was less than 0.3 mm. The errors with regard to the height of the deposited layers mainly come from three sources. Firstly, as indicated by the validation results of the predicted manufacturing parameters (shown in Table 5), the heights of the elementary weld beads belonging to the third and fourth layers were smaller than the expected values. This implies a fact that using the predicted parameters will result in a shortage of height. Secondly, the model used for predicting the manufacturing parameters of elementary weld beads was built by depositing single weld beads on a flat substrate in the room temperature. However, due to the continuous depositions of the weld beads for filling the groove, the heat-dissipation conditions of the actually de-

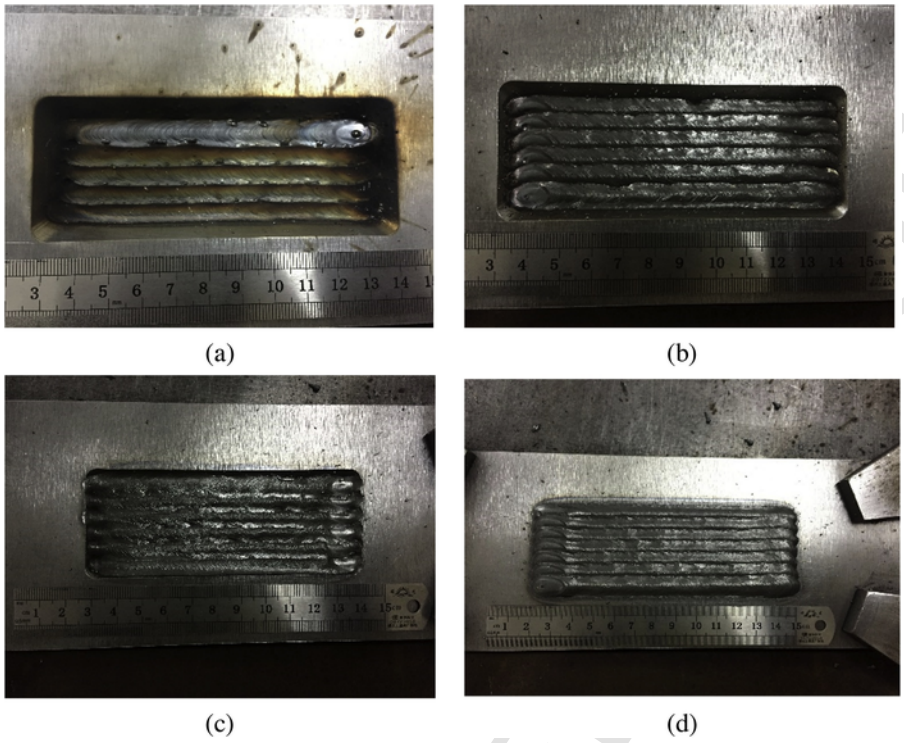

Fig. 11. The forming appearance of (a) The first layer, (b) The second layer, (c) The third layer, and (d) The fourth layer.

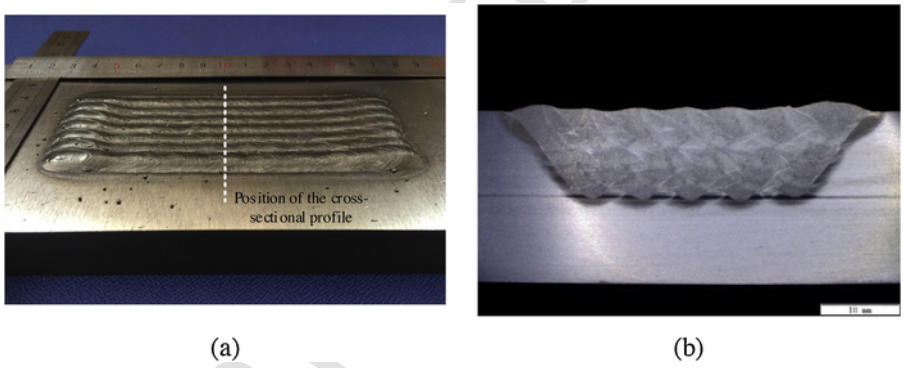

Fig. 12. The repaired part: (a) An overall view of the groove filled by WAAM, (b) The cross-sectional profile of the fabricated part.

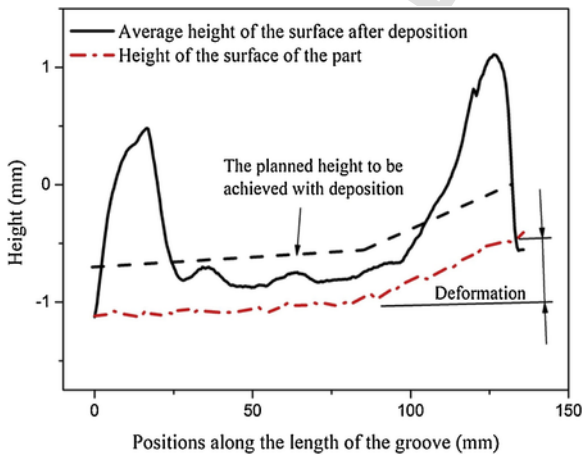

Fig. 13. The result of measurements on the surface of the part after deposition.

posited weld beads were different from the condition in which the model was built. Thus, the solidification time of the actually deposited weld beads was longer than that of the beads in the model. This is the reason why the heights of the actually deposited weld beads were lower than the expected heights. Last but not least, during the deposition process, splash may always happen, which accidentally caused the loss of the fed material.

Another important finding from the experimental results was that the deposition process caused a deformation in the part. A bow-like warping distortion perpendicular to the surface of the part can be observed from Figs. 12(a) and 13. The out-of-plane distortion along the length of the part over 135 mm was 1.2 mm, approximately. The deformation was mainly caused by the shrinkage of weld beads and adjacent base metal during cooling. Since the groove to be filled by WAAM is on a side of the part (asymmetrical structure), the welding-induced stresses are not evenly distributed along the thickness direction of the part. As a result, the warping distortion causes surface unevenness of the repaired part. In addition, due to the deformation, the preplanned paths for conducting the finishing machining operations may become invalid. For these reasons, the generated deformation should be elim-

inated as much as possible before the finishing machining operations can be applied. Possible solutions may include interpass rolling, heat treatment, *etc*.

If the buy-to-fly ratio of the fed material is defined according to the following formula:

$$R_m = \frac{V_g}{V_g + V_r} \tag{21}$$

where V_g is referred to as the volume of the groove, V_r is the volume of the redundant material that needs to be removed through the after-process machining operations. In this case, the ratio of material utilization was calculated as 92.1%. Therefore, due to the careful planning of the manufacturing parameters, a relatively high material utilization was achieved.

Furthermore, preventing the formation of voids between the part and the fed material is one of the major requirements for part repair using WAAM. To validate the effectiveness of the proposed fundamentals concerning this aspect, an X-ray radiographic inspection was taken on the repaired part, which is a nondestructive examination approach. In the test, the supply voltage was 210 kV and the exposure time was 2 min. The photographic film showing the result of the inspection is presented in Fig. 14. In the image quality indicator (IQI) presented at the lower right corner, the diameter of the metal wire for W10 was 0.40 mm, while that for W16 was 0.10 mm. The metal wire with the diameter of 0.32 mm (W11) can be seen from the figure, which means that the required resolution for inspecting a steel plate with the thickness of 200 mm is met according to the technical standard GB/T3323-2005.

It can be observed from the result that no weld porosity, incomplete fusion or crack was produced in the part. The fusion between the striking and distinguishing areas of the welding arc and the machined groove is reasonably good. In addition, several small slag inclusions can be seen, which are randomly distributed in the main body of the groove among weld beads. The quality level of the repaired part can be evaluated as Grade I (the highest grade) according to GB/T3323-2005 standard. It requires that the number of circular defects in any 10*30 mm area should be less than 6 concerning a welded component with a thickness of 100 mm or more. The examination result proved that the fundamentals proposed in this paper effectively achieved a good repair quality concerning the fusion between the part and the fed material.

The main reason for the generated inclusions might be the low heat-input applied for depositing the weld beads. Increasing the heat-input in deposition, such as using a large current or a low speed of deposition, may facilitate the fusion of weld beads. However, significant heat-induced distortions will be generated at the same time. The implication is that the manufacturing parameters of WAAM for part repair should be articulated according to the practical needs, in which trade-off considerations are required to be made.

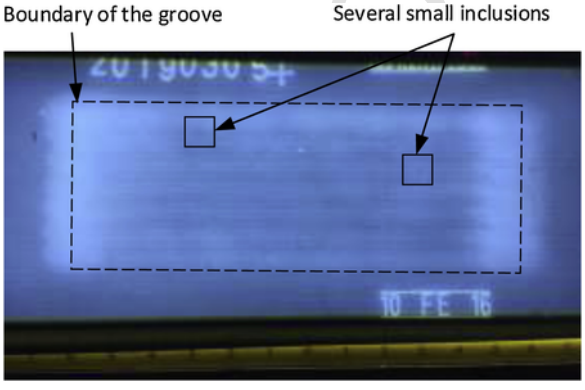

Fig. 14. The result of X-ray radiographic inspection applied on the repaired part.

6. Conclusions and future work

With the objective to support repairing parts with surface defects by machining and WAAM, both theoretical fundamentals and experimental validations are proposed in this paper. Based on the conducted research, the conclusions have been drawn as follows:

- To enable a sufficient fusion between the lateral faces of a groove to be machined on the surface of a worn part and the weld beads deposited by WAAM, the inclination angle of the machined groove should be purposefully calculated. The lower limit of the fabrication range of the inclination angle depends on the height to width ratio of the concerned weld beads, and the step-over rate applied to arrange weld beads in the layers, while the upper limit of the fabrication range depends on the geometries of the weld beads, the diameter of the weld gun, and the applied stick-out distance of the same.
- A mathematical model for WAAM of layers with supportive lateral surfaces was proposed. The relation between the geometries of a given groove (*e.g.* depth, width of the base surface and inclination angle) and the geometries of beads (*i.e.* height and width) used for the filling was carried out. Based on the conducted case study, the model was proofed to be feasible for calculating manufacturing parameters for filling a machined groove by using WAAM.
- The experimental results showed that the manufacturing parameters calculated based on the proposed fundamentals (the criteria and the model) achieved a good repair quality of an assumed worn part. Despite a deformation in the repaired part was caused, high fabrication accuracy and material utilization were achieved. Automatic repairing by integration of machining and WAAM can be realized.

Future research proposals may consider the following aspects. Firstly, based on the proposed fundamentals, an automatic repairing system is about to be implemented. In addition, due to the geometrical deviations of the deposited weld beads to the expected ones, a process control mechanism will be applied to adjust the manufacturing parameters in order to increase the fabrication accuracy. Thirdly, microstructure and mechanical properties of the repaired part will be focused and the impact of different deposition strategies (*e.g.* different path patterns) will be investigated. Last but not least, in this research, the shape of the groove was assumed to be a pyramidal frustum with two rectangular bases. The design principles for determining the optimal shape of the groove concerning different practical requirements need further research investigations.

Declaration of Competing Interest

None.

Acknowledgment

This work was supported by National Key R&D Program of China (2018YFB1105800).

References

Bermingham, M.J., Nicastro, L., Kent, D., Chen, Y., Dargusch, M.S., 2018. Optimising the mechanical properties of Ti-6Al-4V components produced by wire + arc additive manufacturing with post-process heat treatments. J. Alloys Compd. 753, 247–255. https://doi.org/10.1016/j.jallcom.2018.04.158.

Branza, T., Deschaux-Beaume, F., Sierra, G., Lours, P., 2009. Study and prevention of cracking during weld-repair of heat-resistant cast steels. J. Mater. Process. Technol. 209, 536–547. https://doi.org/10.1016/j.jmatprotec.2008.02.033.

Chen, C., Wang, Y., Ou, H., He, Y., Tang, X., 2014. A review on remanufacture of dies and moulds. J. Clean. Prod. 64, 13–23. https://doi.org/10.1016/j.jclepro.2013.09.014.

Chen, X., Su, C., Wang, Y., Siddiquee, A.N., Sergey, K., Jayalakshmi, S., Singh, R.A., 2018. Cold metal transfer (CMT) based wire and arc additive manufacture (WAAM) system. J. Synch. Investig. 12, 1278–1284. https://doi.org/10.1134/S102745101901004X.

Ding, D., Pan, Z., Cuiuri, D., Li, H., 2015. A multi-bead overlapping model for robotic wire and arc additive manufacturing (WAAM). Rob. Comput. Integr. Manuf. 31, 101–110. https://doi.org/10.1016/j.rcim.2014.08.008.

Ding, D., Pan, Z., Cuiuri, D., Li, H., 2015. Wire-feed additive manufacturing of metal components: technologies, developments and future interests. Int. J. Adv. Manuf. Technol. 81, 465–481. https://doi.org/10.1007/s00170-015-7077-3.

Ding, D., Shen, C., Pan, Z., Cuiuri, D., Li, H., Larkin, N., van Duin, S., 2016. Towards an automated robotic arc-welding-based additive manufacturing system from CAD to finished part. Comput. Aided Des. 73, 66–75. https://doi.org/10.1016/j.cad.2015.12.003.

Flynn, J.M., Shokrani, A., Newman, S.T., Dhokia, V., 2016. Hybrid additive and subtractive machine tools – research and industrial developments. Int. J. Mach. Tools Manuf. 101, 79–101. https://doi.org/10.1016/j.ijmachtools.2015.11.007.

Graf, B., Gumenyuk, A., Rethmeier, M., 2012. Laser metal deposition as repair technology for stainless steel and titanium alloys. Phys. Procedia 39, 376–381. https://doi.org/10.1016/j.phpro.2012.10.051.

Hönnige, J.R., Colegrove, P.A., Ganguly, S., Eimer, E., Kabra, S., Williams, S., 2018. Control of residual stress and distortion in aluminium wire + arc additive manufacture with rolling. Addit. Manuf. 22, 775–783. https://doi.org/10.1016/j.addma.2018.06.015.

Horgar, A., Fostervoll, H., Nyhus, B., Ren, X., Eriksson, M., Akselsen, O.M., 2018. Additive manufacturing using WAAM with AA5183 wire. J. Mater. Process. Technol. 259, 68–74. https://doi.org/10.1016/j.jmatprotec.2018.04.014.

Karunakaran, K.P., Suryakumar, S., Pushpa, V., Akula, S., 2009. Retrofitment of a CNC machine for hybrid layered manufacturing. Int. J. Adv. Manuf. Technol. 45, 690–703. https://doi.org/10.1007/s00170-009-2002-2.

Knezović, N., Topić, A., 2018. Wire and arc additive manufacturing (WAAM)–A new advance in manufacturing. In: In: Karabegović, I. (Ed.), New Technologies, Development and Application, vol. 42, Lecture Notes in Networks and Systems, pp. 65–71. https://doi.org/10.1007/978-3-319-90893-9_7.

Lant, T., Robinson, D.L., Spafford, B., Storesund, J., 2001. Review of weld repair procedures for low alloy steels designed to minimise the risk of future cracking. Int. J. Pres. Ves. Pip. 78, 813–818. https://doi.org/10.1016/S0308-0161(01)00094-1.

Li, Y., Han, Q., Zhang, G., Horváth, I., 2018. A layers-overlapping strategy for robotic wire and arc additive manufacturing of multi-layer multi-bead components with homogeneous layers. Int. J. Adv. Manuf. Technol. 96, 3331–3344. https://doi.org/10.1007/s00170-018-1786-3.

Li, Y., Huang, X., Horváth, I., Zhang, G., 2018. GMAW-based additive manufacturing of inclined multi-layer multi-bead parts with flat-position deposition. J. Mater. Process. Technol. 262, 359–371. https://doi.org/10.1016/j.jmatprotec.2018.07.010.

Li, Y., Sun, Y., Han, Q., Zhang, G., Horváth, I., 2018. Enhanced beads overlapping model for wire and arc additive manufacturing of multi-layer multi-bead metallic parts. J. Mater. Process. Technol. 252, 838–848. https://doi.org/10.1016/j.jmatprotec.2017.10.017.

Liu, D., Lippold, J.C., Li, J., Rohklin, S.R., Vollbrecht, J., Grylls, R., 2014. Laser engineered net shape (LENS) technology for the repair of Ni-base superalloy turbine components. Metall. Mater. Trans. A 45, 4454–4469. https://doi.org/10.1007/s11661-014-2397-8.

Panchagnula, J.S., Simhambhatla, S., 2016. Inclined slicing and weld-deposition for additive manufacturing of metallic objects with large overhangs using higher order kinematics. Virtual Phys. Prototyp. 11, 99–108. https://doi.org/10.1080/17452759.2016.1163766.

Penaranda, X., Moralejo, S., Lamikiz, A., Figueras, J., 2017. An adaptive laser cladding methodology for blade tip repair. Int. J. Adv. Manuf. Technol. 92, 4337–4343. https://doi.org/10.1007/s00170-017-0500-1.

Pikuła, J., Łomozik, M., Pfeifer, T., 2017. The influence of manual metal arc multiple repair welding of long operated waterwall on the structure and hardness of the heat affected zone of welded joints. Arch. Metall. Mater. 62, 327–333. https://doi.org/10.1515/amm-2017-0049.

Rajkolhe, R., Khan, J., 2017. Defects, causes and their remedies in casting process: a review. Int. J. Res. Adv. Technol. 2, 375–383.

Ren, L., Eiamsa-ard, K., Ruan, J., Liou, F., 2007. Part repairing using a hybrid manufacturing system. Georgia, USA, October 15–18. ASME 2007 International Manufacturing Science and Engineering Conference Atlanta 1–8. https://doi.org/10.1115/MSEC2007-31003.

Song, Y.A., Park, S., Choi, D., Jee, H., 2005. 3D welding and milling: part I–a direct approach for freeform fabrication of metallic prototypes. Int. J. Mach. Tools Manuf. 45, 1057–1062. https://doi.org/10.1016/j.ijmachtools.2004.11.021.

Suryakumar, S., Karunakaran, K.P., Bernard, A., Chandrasekhar, U., Raghavender, N., Sharma, D., 2011. Weld bead modeling and process optimization in hybrid layered manufacturing. Comput. Aided Des. 43, 331–344. https://doi.org/10.1016/j.cad.2011.01.006.

Wang, J., Prakash, S., Joshi, Y., Liou, F., 2002. Laser aided part repair-a review. Austin, TX. Citeseer. Proceedings of the Thirteenth Annual Solid Freeform Fabrication Symposium 57–64.

Wilby, A., Neale, D., 2009. Defects introduced into metals during fabrication and service. Mater. Sci. Eng. 3, 48–75.

Williams, S.W., Martina, F., Addison, A.C., Ding, J., Pardal, G., Colegrove, P., 2016. Wire + arc additive manufacturing. Mater. Sci. Technol. 32, 641–647. https://doi.org/10.1179/1743284715Y.0000000073.

Wu, B.T., Pan, Z.X., Ding, D.H., Cuiuri, D., Li, H.J., Fei, Z.Y., 2018. The effects of forced interpass cooling on the material properties of wire arc additively manufactured Ti6Al4V alloy. J. Mater. Process. Technol. 258, 97–105. https://doi.org/10.1016/j.jmatprotec.2018.03.024.

Xiong, J., Lei, Y., Chen, H., Zhang, G., 2017. Fabrication of inclined thin-walled parts in multi-layer single-pass GMAW-based additive manufacturing with flat position deposition. J. Mater. Process. Technol. 240, 397–403. https://doi.org/10.1016/j.jmatprotec.2016.10.019.

Xiong, J., Yin, Z., Zhang, W., 2016. Forming appearance control of arc striking and extinguishing area in multi-layer single-pass GMAW-based additive manufacturing. Int. J. Adv. Manuf. Technol. 87, 579–586. https://doi.org/10.1007/s00170-016-8543-2.

Xiong, J., Zhang, G., Gao, H., Wu, L., 2013. Modeling of bead section profile and overlapping beads with experimental validation for robotic GMAW-based rapid manufacturing. Rob. Comput. Integr. Manuf. 29, 417–423. https://doi.org/10.1016/j.rcim.2012.09.011.

Xiong, J., Zhang, G., Hu, J., Li, Y., 2013. Forecasting process parameters for GMAW-based rapid manufacturing using closed-loop iteration based on neural network. Int. J. Adv. Manuf. Technol. 69, 743–751. https://doi.org/10.1007/s00170-013-5038-2.

Xiong, J., Zhang, G., Hu, J., Wu, L., 2014. Bead geometry prediction for robotic GMAW-based rapid manufacturing through a neural network and a second-order regression analysis. J. Intell. Manuf. 25, 157–163. https://doi.org/10.1007/s10845-012-0682-1.

Yilmaz, O., Gindy, N., Gao, J., 2010. A repair and overhaul methodology for aeroengine components. Rob. Comput. Integr. Manuf. 26, 190–201. https://doi.org/10.1016/j.rcim.2009.07.001.

Yu, J.H., Choi, Y.S., Shim, D.S., Park, S.H., 2018. Repairing casting part using laser assisted additive metal-layer deposition and its mechanical properties. Opt. Laser Technol. 106, 87–93. https://doi.org/10.1016/j.optlastec.2018.04.007.

Zhang, X., Krewet, C., Kuhlenkötter, B., 2006. Automatic classification of defects on the product surface in grinding and polishing. Int. J. Mach. Tools Manuf. 46, 59–69. https://doi.org/10.1016/j.ijmachtools.2005.03.013.